INDC(USA)-108
Distr. ST/J/RD

IAEA
International Atomic Energy Agency

# INDC International Nuclear Data Committee

# VERIFICATION OF THE $^{252}$CF STANDARD IN THE ENERGY RANGE 2 – 20 MEV

N.V. Kornilov

9 Bolleana Pl, Athens, OH, 45701, USA

July 2015

IAEA Nuclear Data Section
Vienna International Centre, P.O. Box 100, 1400 Vienna, Austria

Selected INDC documents may be downloaded in electronic form from
*http://www-nds.iaea.org/publications*
or sent as an e-mail attachment.
Requests for hardcopy or e-mail transmittal should be directed to
*NDS.Contact-Point@iaea.org*
or to:
Nuclear Data Section
International Atomic Energy Agency
Vienna International Centre
PO Box 100
1400 Vienna
Austria

Printed by the IAEA in Austria

July 2015

**INDC(USA)-108**
**Distr. ST/J/RD**

# Verification of the $^{252}$Cf Standard in the Energy Range 2 – 20 MeV

N.V. Kornilov

9 Bolleana Pl, Athens, OH, 45701, USA

Final Report of an IAEA Research Contract

## ABSTRACT

The dynamic threshold method was applied for investigation of the $^{252}$Cf PFNS. The spectrum was measured with reasonable accuracy in the energy range 2 - 20 MeV for the first time. A double goal task was proclaimed and was solved. From one side it is very interesting to verify the $^{252}$Cf standards in the whole energy range < 20 MeV. From another side, the results measured with a new approach in comparison with well-known standards may give additional information about the accuracy of the new method. Results of the data analysis are collected in this report.

July 2015

## Contents

# 1. Introduction

The application of a standard neutron source with reasonably high intensity in the whole energy range up to 20 MeV is a unique possibility for measurement of neutron detector efficiency with high accuracy. This approach may simplify the investigation of different neutron spectra.

In 1986, the neutron standard spectrum was suggested by Mannhart [1] on the basis of the spontaneous neutron fission of $^{252}$Cf. This standard has obvious advantages and disadvantages.

Advantages:

1. The neutron source with timing of fission fragments for time of flight experiments (FWHM = 1 - 2 ns) is a rather simple device which may be realized in any nuclear physics laboratory.
2. The fission count rate ~ $10^5$ 1/s allows to measure the efficiency of a traditional neutron detector on the basis of a hydrogen scintillator during ~ 100 h with statistical uncertainties comparable with errors of standard spectra (1-3% for energy range 1-10 MeV).

Disadvantages:

1. The rather small life-time. This is defined by the decay time of Cf and transmission of Cf isotopes from "small spot on electrode" in the beginning on the total internal surface of fission fragment counter. The last factor complicates the proper total integration of Fission Fragments (FF) and may destroy the "standard spectrum".
2. The neutron intensity with energy > 10 MeV is very small for fruitful application.
3. The spectrum in the energy range 10 – 20 MeV is practically unknown.

Increasing the accuracy of $^{252}$Cf standard in the energy range 10-20 MeV is still an open problem. This does not only concern the practical application (the low intensity complicates any application in this energy range), but also the investigation of the mechanism of neutron emission in fission. This is a very important task, which is stimulated by two questions: 1) Can the shape of the Prompt Fission Neutron Spectrum be predicted in the frame of a traditional model? 2) Is there any structure in the PFNS shape connected with limits of excitation energy (close to total excitation energy)?

The "bumps" in the PFNS shape were visible in [2] for $^{235}$U at incident energy 0.5-3 MeV. Is this structure reality or not?  Does a similar structure exist for $^{252}$Cf?

The measurement of neutron detector efficiency in the energy range above 10 MeV is a very difficult experimental problem which has not yet been solved. The traditional approach with the application of any standard neutron spectrum does not work. There are no such reference spectra available now (First Research Coordination Meeting on Testing and Improving the International Reactor Dosimetry and Fusion File, IAEA report INDC(NDS)-0639 and https://www-nds.iaea.org/IRDFFtest/). The measured spectra do not have the required accuracy.

The method based on application of symmetric reaction A(A,n)2A-1 does not work. Many symmetric reactions were investigated recently [3]. The conclusion was done that the yield of "mono-energetic neutron" is very small to reach energy ~20 MeV. The only D(d,n) reaction for $E_d$ ~ 15 MeV may be applied (?) for this investigations. However, this experiment was not realized yet.
Reaction of (n,p) scattering which is the main process in the hydrogen neutron detector is the standard. This fact stimulated the Monte Carlo simulation of neutron interaction with a detector and estimation of its efficiency. However, there are some obstacles to the realization of these calculations with high accuracy.

The contribution of (n,α) (Q = -5.7 MeV) reaction at neutron energy > 10 MeV relative to (n,p) scattering is ~ 10%. The alpha particle produces a small pulse height just near the detector threshold or less. The light output for the alpha particle is unknown. The second problem is the scattering in the detector environment. The estimation of the intensity of this process and neutron angular energy distribution is a rather difficult task. Thus the extrapolation of the MC calculation to neutron energy ~ 20 MeV can be done with accuracy not less than ~ 10%, or even higher.

So, we do not have any experimental methods to measure neutron detector efficiency in the energy range up to 20 MeV with high accuracy. Can we suggest a new idea, realize a new method to increase the accuracy in the calculating procedure? It seems a positive answer was given in [4].

So the goal of this investigation is:

- to verify the $^{252}$Cf standards in the whole energy range < 20 MeV.
- to get additional information on the accuracy of the new method by comparing the measured results from the new approach with the well-known standard.

## 2. DYnamic THreshold method (DYTH method) as a unique approach to neutron spectroscopy in the energy range up to 20 MeV with highest accuracy

The method of the dynamic threshold was developed for the NE-213 detector and was investigated using the $^{252}$Cf neutron source. “A dynamically biased neutron detector” was suggested in 1971 [5] for background reduction in TOF experiments. Our realization and motivation are very different. The successful realization of this method is not possible without experimental knowledge of the light output function of the particular detector.

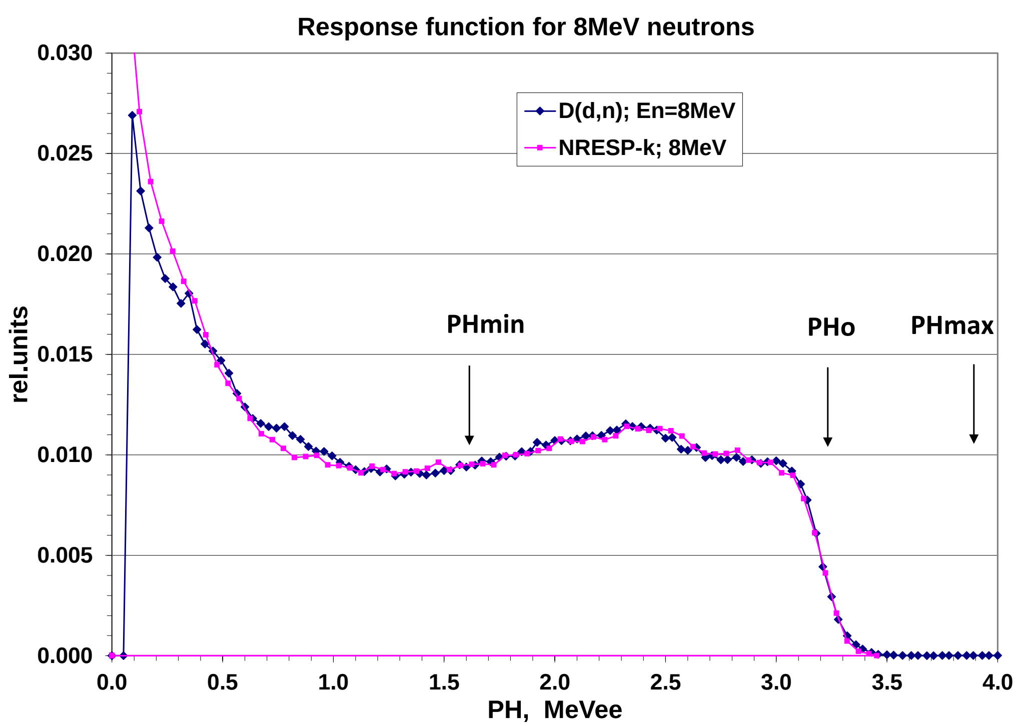


***Fig.1**: Experimental and calculated RF (pulse height distribution) for “monoenergetic neutrons”.*

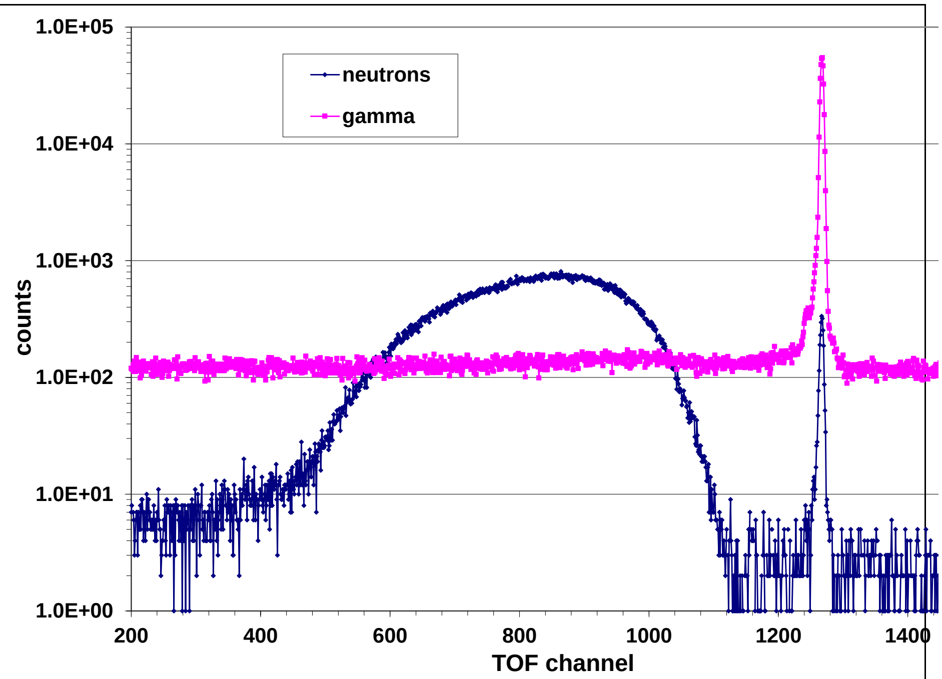


***Fig. 2:*** *TOF distributions without an additional selection.*

Modern techniques allow us to collect all detected events in list mode. So each event is available for off-line analysis. For the realization of this method we should have the following information for each event: time-of-flight (TOF), pulse height (PH), and pulse shape (PS). After the traditional neutron-gamma selection we may analyse only neutron events.

A summary of what is the response function (RF) for the traditional NE213 detector is given in the following. The experimental and calculated RF for 8 MeV neutrons produced with the D(d,n) reaction is shown in Fig.1. The calculation was made with the code developed in PTB (NRESP) [6], and modified in [7]. For the DYTH method, an additional selection of counted events compared with the traditional method, is required. We need the following information (or a method for calculations) for $PH_0$, $PH_{min}$, and $PH_{max}$.

- $PH_0$ is the highest proton energy for selected neutron energy *E*, $PH_0 = L(E)$ – where L(E) is proton light output, and E is energy estimated from TOF.
- $PH_{min} = E*\cos(\theta)^2$.
- $PH_{max} = PH_0 + 3*\sigma(PH_o)$.

The angle θ may be selected in such a way to remove all unwanted events. In this analysis $\theta = 45^o$ was used.

The selection of events for each neutron energy was made with a simple equation:

$$\text{PHmin} < L < \text{PHmax} \qquad (1)$$

The light output data were measured with "white neutron spectra" and were fitted with function 2 [7] for practical applications:

$$L(E) = (ao + a1 * E)\frac{E^2}{E+Eo} \qquad (2)$$

Where $a_0$,$a_1$, $E_0$ are fitted parameters. The $a_1$ parameter is mainly connected with non-linearity of electron pulses (saturation in PM tube). However, function 2, and fitted parameters are semi-empirical values. Parameters are strongly correlated with each other, so the physical interpretation of all these parameters is a rather difficult task (if possible at all).
The pulse height resolution function was measured in the same experiment, and was described in Eq. 3, with fitted parameters α, β, γ:

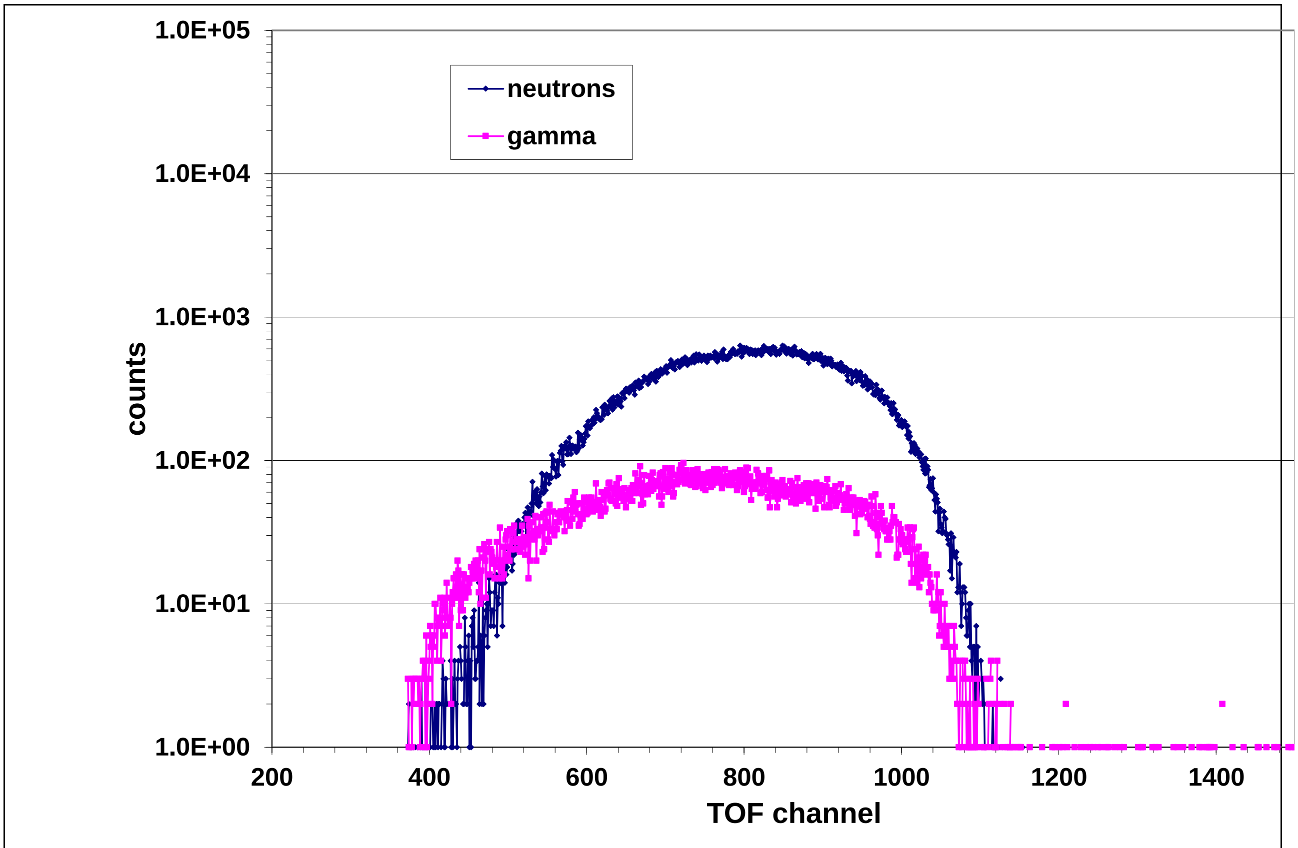


***Fig.3.:*** *TOF spectra for total DYTH method selection: cos(θ)=0.707, and* $PH_{max}=PH_0+3*\sigma(PH_o)$.

$$\sigma = L\left(\alpha^2 + \frac{\beta^2}{L} + \left(\frac{\gamma}{L}\right)^2\right)^{0.5} \qquad (3)$$

The resolution function is a very important parameter for MC simulation in the energy range En < 2 MeV. Calculated results are sensitive to the absolute value and energy dependence of σ(L).

It is worthwhile to note how the incorporation of the DYTH method impacts on the measured TOF distributions. The background events treated as "neutron events" in the time interval between prompt γ-rays and fission neutrons ( > 1100 channels) are removed completely (see Figs 2, 3).

Therefore, advantages of the DYTH method are:
- considerable reduction of the background;
- increase of time resolution (only high PH are used for each neutron energy);
- allowing to remove the main part of the C(n,p), C(n,α) reaction and, as a consequence, allowing to predict the efficiency of the detector with higher accuracy.

Of course we should "pay" for these advantages. The DYTH method reduces the number of counting protons for each input neutron energy, hence it reduces the counting efficiency. The practical application of this method is the goal of this investigation.

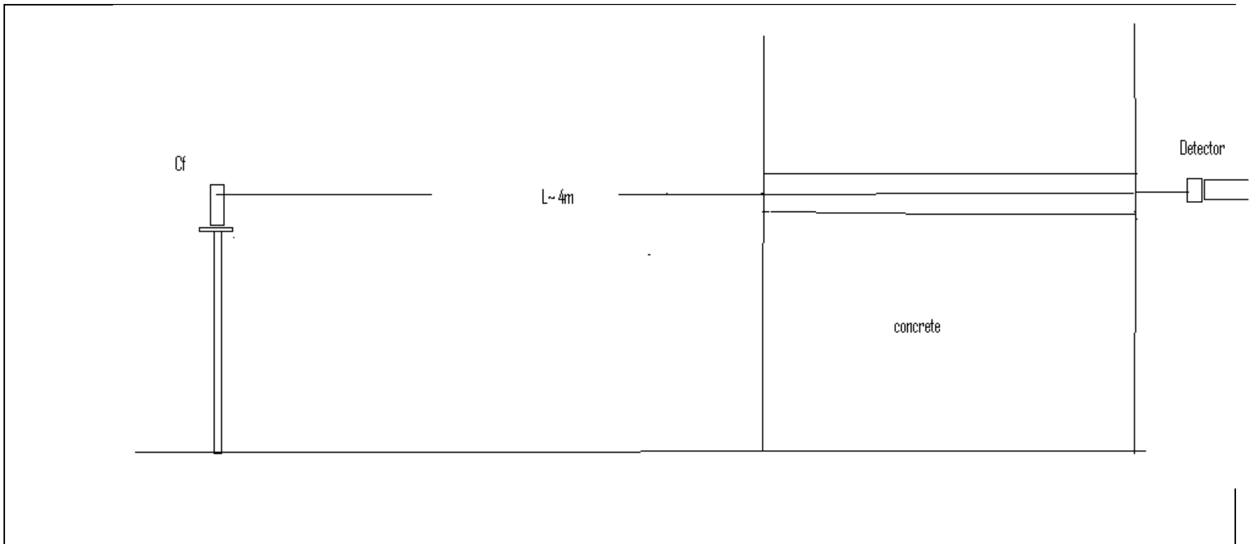


***Fig.4:*** *The experimental set-up. Wall thickness is 1.24m (high density concrete).*

## 3. Cf experiments (neutron source for TOF experiment, neutron detectors)

The experiment is illustrated in Fig.4. Cf-source has the same construction as in paper [7]. Fission Fragments were counted in the fast ionisation chamber. A 3-dimensional sketch of the ionisation chamber is shown in Fig. 5. The Cf layer (Ø = 10 mm) was placed on a polished stainless steel electrode (Ø = 25 mm). The wall thickness of the chamber (stainless steel) is 0.2 mm. All massive parts were moved far away from the source. The chamber was filled with an Ar+10%$C0_2$ mixture up to ~ 1.2 bar.
The fast current pre-amplifier, fast amplifier, and Constant Fraction Discriminator (CFD) provide "stop signal". The threshold of CFD was adjusted in such way as to provide high efficiency of FF counting (~ 99%).

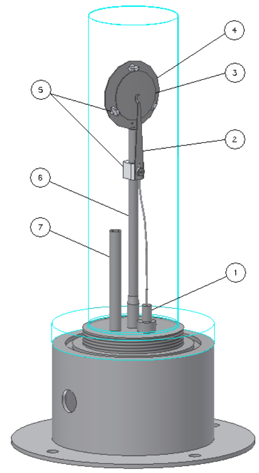


***Fig.5****: Drawing of the ionisation chamber for the $^{252}$Cf reference source.*
*1- high voltage, output signal, 2 – contactor, 3- $^{252}$Cf layer , 4 – collecting electrodes,*
*5 – insulators, 6 – holder (thin walled tube), 7 – gas inlet.*

The detector consists of a NE213 scintillator with diameter 12.7 cm and height 5.08 cm. The scintillator is coupled to a photomultiplier tube, RCA 4522, with a 12.7 cm diameter photo cathode [8]. After splitting the anode signal with a T-splitter, part of the signal was used for timing and the other part for neutron-gamma discrimination. The threshold for a constant fraction discriminator in the timing channel was adjusted to ~ 30 keVee (half of the $^{241}$Am gamma-ray pulse height). The second part of the anode pulse was fed to a MESYTEC unit [9].

The 10$^{th}$ (8$^{th}$ for run 3, or anode for run 1) dynode signal after the pre-amplifier and spectroscopic amplifier was applied for measurement of the pulse height distribution. All events were collected in list-mode. The bias (detector efficiency), and "cut" for neutron-gamma discrimination were adjusted off line. Any part of events can be selected for checking of the gain in the linear channel. Any additional selection required by the DYTH method may be realized without any problem.

Experimental parameters are listed in Table 1.

Table 1. Parameters of experiments used for Cf spectrum investigations. Uncertainties for L – dL ~ 0.5 cm, uncertainty for τ (TOF channel width) was ~ 0.1%. Total time of experiments was 4520.1 h.

| Experiments | Cf, 1/s | Light output | L, m | τ, ns | amount of "short runs" | Total time, h |
|---|---|---|---|---|---|---|
| Run 1, Aug-Dec 2009 | $2.9\cdot10^4$ | Al(d,n) | 4.108 | 0.2085 | 3 | 170.5 |
| Run 3, Nov 2010-Feb 2011 | $3.9\cdot10^4$ | Cf(E) | 4.229 | 0.2301 | 18 | 1143.6 |
| Run 5, Apr - Jul 2012 | $2.8\cdot10^4$ | Cf(E) | 4.114 | 0.2165 | 29 | 1344.1 |
| Run 7, Apr - Jun 2013 | $2.2\cdot10^4$ | Cf(E) | 4.238 | 0.2174 | 22 | 1861.9 |

The same source (Cf layer) was applied in Runs 3-7. So it is interesting to compare the absolute count rate estimated for "each short run" with the general tendency of Cf decay. All "Cf activity data" are shown in Fig. 6. The measured uncertainty for each "short run" was ~ 0.5 %. The systematic data shift relative to the common decay line is ~ 1 %. So, one can conclude that we fixed the $^{252}$Cf fission activity, and measured this activity with uncertainties ~ 1 %.

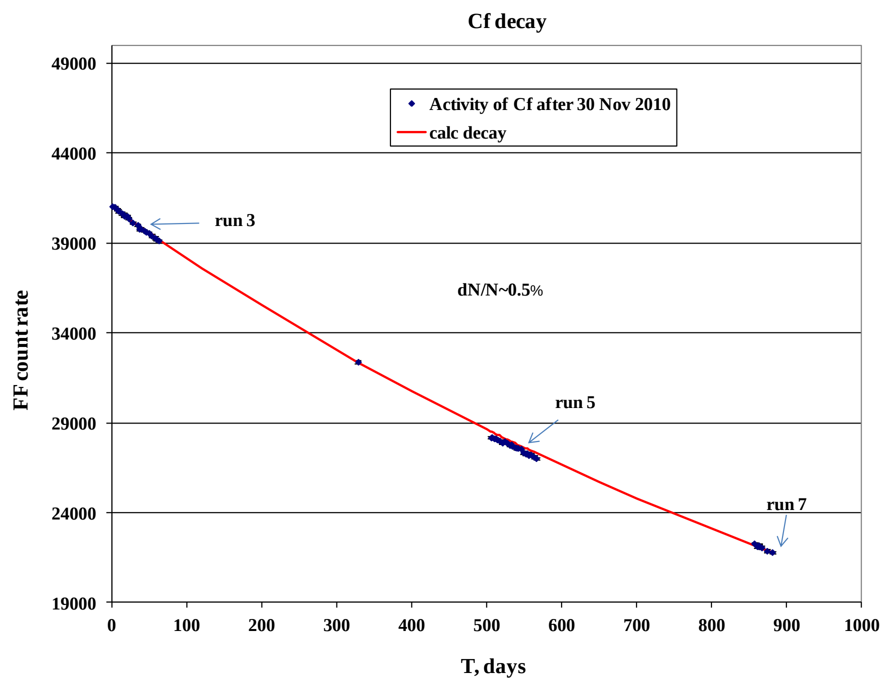


***Fig.6**: Cf activity and measured points for runs 3,5,and 7.*

Light outputs, and energy resolution functions were measured relative to "white neutron spectra": Al(d,n) neutrons for Run 1, and PFNS for $^{252}$Cf for other Runs. Finally, the experimental Cf fission neutron spectrum was compared with the "standard spectrum", but the information about the Cf spectrum shape was not used (nowhere in this work) for estimation of the detector efficiency.

## 4. Electron energy scale calibration

The calibration of the PH scale for electron energy was submitted to the International Conference on Nuclear Data for Science and Technology (ND2013) [10]. Gamma-sources, gamma-rays and electron energies, and the method of the channel number estimation are listed in Table 2.

Table.2 Parameters for scale calibration

| Source | $E_\gamma$, MeV | $E_e$, MeV | position |
|---|---|---|---|
| $^{22}$Na | 0.511 | 0.34 | 1 |
| $^{207}$Bi | 0.57 | 0.393 | 1 |
| $^{137}$Cs | 0.662 | 0.477 | 1 |
| $^{207}$Bi | 1.064 | 0.857 | 1 |
| $^{22}$Na | 1.275 | 1.061 | 1 |
| $^{207}$Bi | 1.77 | 1.547 | 1 |

| Source | $E_\gamma$, MeV | $E_e$, MeV | position |
|---|---|---|---|
| np-capture | 2.225 | 1.995 | 1 |
| $^{208}Tl$(Th chain) | 2.615 | 2.381 | 1 |
| $^{12}C$ | 4.438 | 3.416 | 2 |
| $^{12}C$ | 4.438 | 4.2 | 3 |

The channel number N, which corresponds to the electron energy given in Table 2, was estimated by comparing experimental spectra with Monte Carlo simulations. The energy deposited in the scintillator from an isotropic point source was modeled with GEANT-4.

The numbers in the last column mean: 1- Compton effect $N = (N_{max}+N_{1/2})/2$ [6]; 2 - pair production, $E_e = E_\gamma-2mc^2$, $N=N_{max}$ in the first peak. 3- pair production. $E_e$ = 4.2MeV, $N = N_{0.75}$. An energy spectrum obtained from a Pu(Be) source depicting the neutron component and high-energy gamma rays is given in Fig. 7.

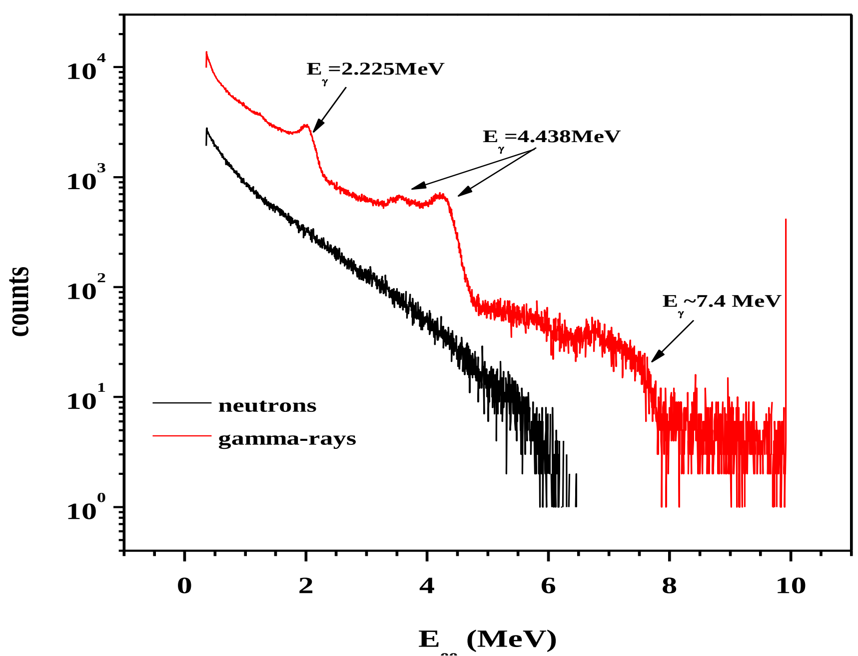


***Fig.7:*** *Experimental pulse-height spectra for Pu(Be) source.*

Experimental and calculated spectra for the 4.438 MeV gamma ray are given in Fig. 8. The calculated data are shown with and without energy resolution convolution.
Following [7], non-linear light output L(E) for electrons was assumed:

$$L = \frac{E_e^{\ 2}}{E_e + E_0},\ [E_e], [L]=\text{MeV},\ E_0=0.034\text{MeV} \tag{4}$$

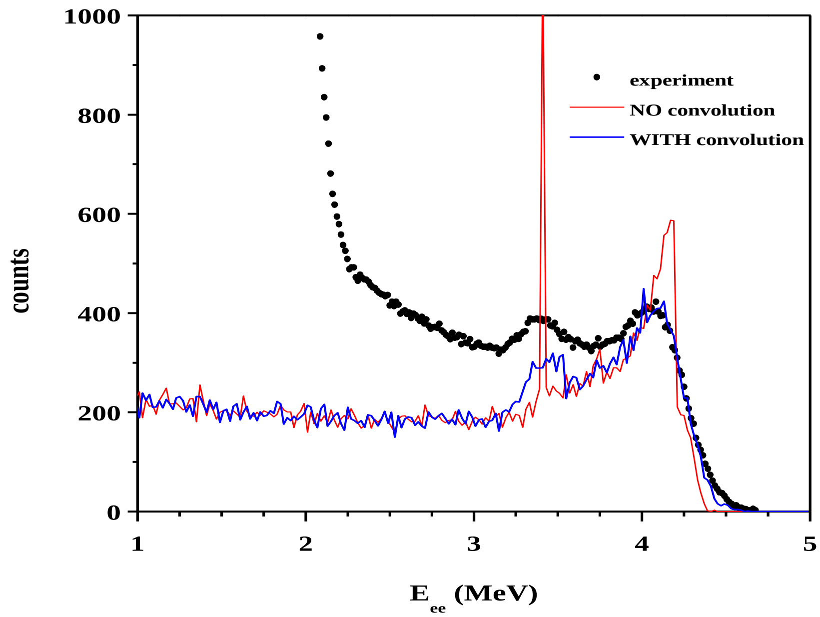


***Fig.8:*** *Experimental and calculated spectra for 4.438 MeV gamma-rays.*

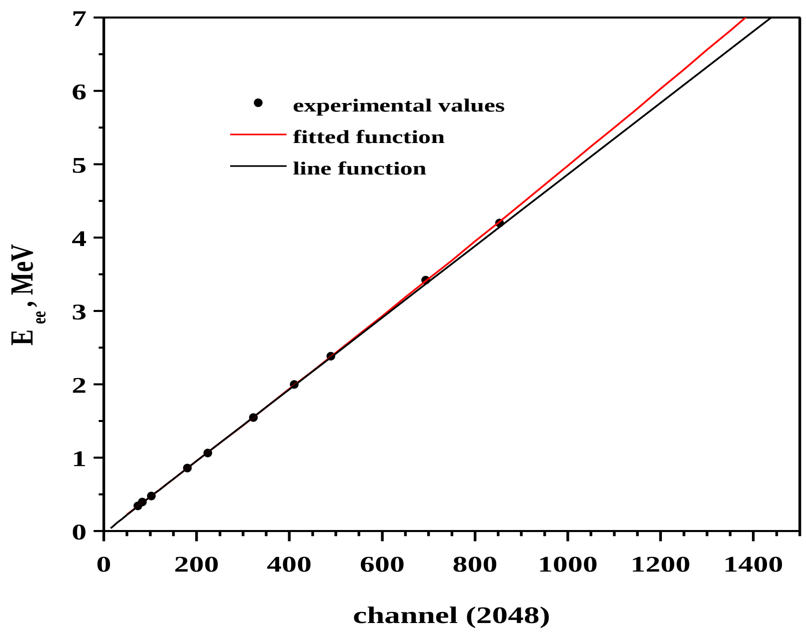


***Fig.9:*** *Electron light output calibration*

The dependence of the light output versus the channel number N was described by a quadratic function. This function, with fitting parameters together with a linear fit below $E_e < 2$ MeVee and experimental data from one of the detectors, is shown in Fig. 9.

The fitted function was extrapolated to ~ 7MeVee and compared with the edge of the spectrum calculated with GEANT-4 code. The contribution of gamma-rays with energies 7.545 MeV and 6.862 MeV ($^9$Be(α,γ) reaction) is unknown for Pu(Be) source. It was assumed that weights are 0.8 and 0.2. The agreement between calculated and experimental data (spectrum edge) is very good (Fig.10).

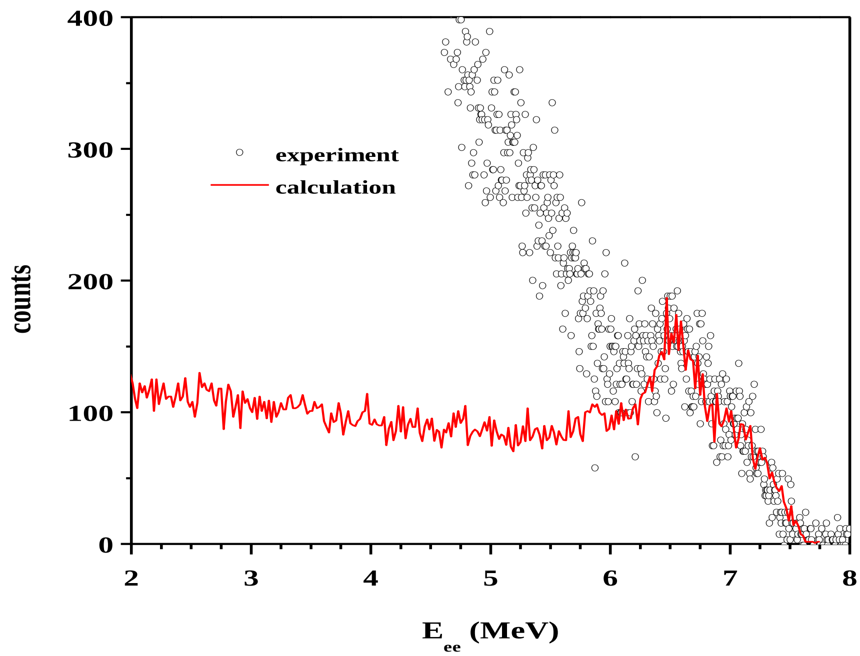


***Fig.10:*** *Experimental and calculated spectra in ~7MeVee region.*

## 5. Stability of the detector operation

This experiment was very time consuming. The total time to carry out all Runs was ~ 190 days. Thus, it is important to verify detector stability. We used the off-line analysis to check the stability of the detector and incorporate proper correction if necessary. The $^{252}$Cf PH spectrum (together with background) was measured during several months together with TOF data. During this run time the pulse height spectra for $^{207}$Bi was also measured. The spectra measured during the current run $S(Y)$ were compared with a reference spectrum $S(X)$ with following equation.

$$\chi^2 = \sum_{i=1}^{n} \frac{\left(S(X_i) - a_0 S(Y_i)\right)^2}{\sigma^2} \tag{5}$$

where $X_i$ is the channel number for the reference spectrum, $Y_i=a_1+a_2*X_i$ the channel number for the current run, $a_0$ the normalization parameter. In addition, the high voltage was checked during the whole experiment by means of a digital voltmeter. Parameters $a_i$ were found by the non-linear Least Square Method.

Table 2. Fitted parameters and their uncertainties for several "short runs" during run 7.

| #Short run | $a_2$ | $\delta a_2/a_2$ | $a_1$ | $\delta a_1/a_1$ | $\chi^2$ |
|---|---|---|---|---|---|
| 1 | 1.0167 | 3.6e-4 | -0.63 | 0.17 | 1.70 |
| 2 | 0.9909 | 3.3e-4 | -0.42 | 0.22 | 1.49 |
| 3 | 0.9931 | 3.8e-4 | 0.59 | 0.19 | 1.56 |
| 4 | 0.9996 | 3.5e-4 | -0.55 | 0.19 | 1.40 |

Fitted parameters and their uncertainties are listed in Table 2. The gain of the detector may be estimated with accuracy ~ 0.04 %. The non-stability of ~ 1.7 % is visible and may be reduced using the suggested method, as shown in Fig.11.

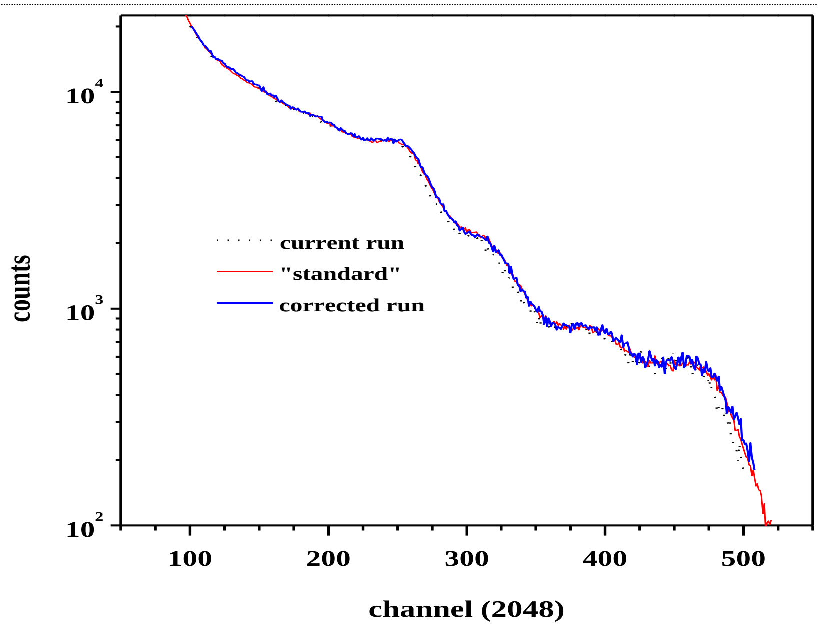


***Fig. 11:*** *PH for $^{252}Cf$ and BGR. Reference spectrum and current run after fitting procedure are given (gain correction 1.67 %).*

As a rule, $a_2$ parameters were very close to unity. However, sometimes the difference increased up to 10-15 %. The temperature in the tunnel, and the high voltage for the detector were the same. The spectrum shape also changed, not only amplification.

This "puzzle" took a long time and was not easily resolved. Finally, the answer was very simple. This "unstability effect" was artificial. When the accelerator started operation, the door in the tunnel was closed and the door moved closer to the neutron detector. It was an extra source of gamma-rays due to neutron activation. This fact explains the changing of the PH spectrum shape.

The fan was placed at the end of the tunnel, to avoid overheating. When the door was closed, the air flow through the collimator increased considerably. In our case the detector was placed rather close to the exit of the collimator. This extra air flow reduced temperature of the detector, and changed the gain of PMT.

When this "source of instability" was fixed, there were no other problems with the stability of the detector. The "off-line" procedure for amplification checking was applied for each "short run". But as a rule the gain was not changed more than ~ 1 %.

## 6. Experimental light output L(E) and PH resolution functions. L(E) peculiarities

The time-of-flight method for measurement of L(E) was discussed in [7]. After proper calibration of PH scale we select "monoenergetic" neutrons by TOF method. And finally, the matrix of the RF shown in Fig. 1 may be constructed for wide energy range. The upper energy limit is connected with intensity of the neutrons at high energy. The following analysis of this RF matrix gives us the average energy of the edge (electron energy corresponding to protons), dispersion of electron energy (slope of the edge). The method and procedure of data evaluation may be found in [7].

The analytical function 2 was fitted to experimental L(E) points. Parameters for all runs are collected in table 3. In this investigation the energy range for L(E) estimation was 1.5 - 12 MeV.

Table 3. Fitted parameters for L(E) function. $a_1 = 0.005$ parameter was fixed for Runs 5,7

| Run | $a_o$ | $a_1$ | $E_0$, MeV | $\chi^2$ |
|---|---|---|---|---|
| Run 1 | 1.105±0.146 | -(0.034±0.008) | 8.76±1.58 | 0.18 |
| Run 3 | 0.700±0.049 | 0.007±0.003 | 3.18±0.38 | 0.46 |
| Run 5 | 0.630±0.008 | 0.005 | 2.21±0.11 | 0.22 |
| Run 7 | 0.623±0.009 | 0.005 | 2.15±0.11 | 0.21 |

The experimental data and fitted function for Runs 1,5 are shown in Fig. 12. The difference between Run 1 and Run 5 is visible and (seems) connected with the fact that linear output for PH measurements was taken from anode (Run 1) and $10^{th}$ dynode (Run 5).

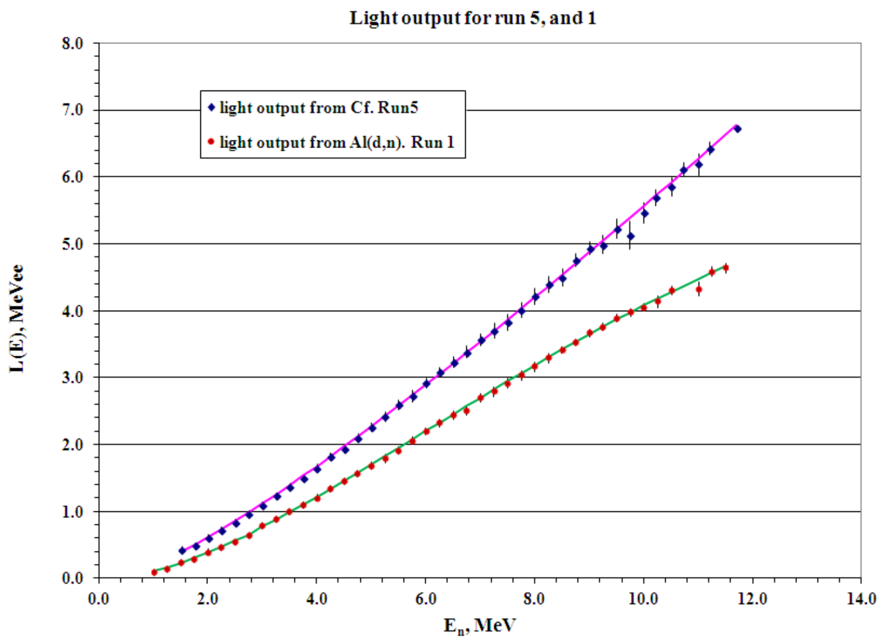


***Fig. 12****: Light output for run 1, and run3. Lines show fitted function*

The saturation of the anode pulse provides non-linearity for all pulses (electron and protons). As a consequence, we have a very big, negative term $a_1$ for the anode pulses.

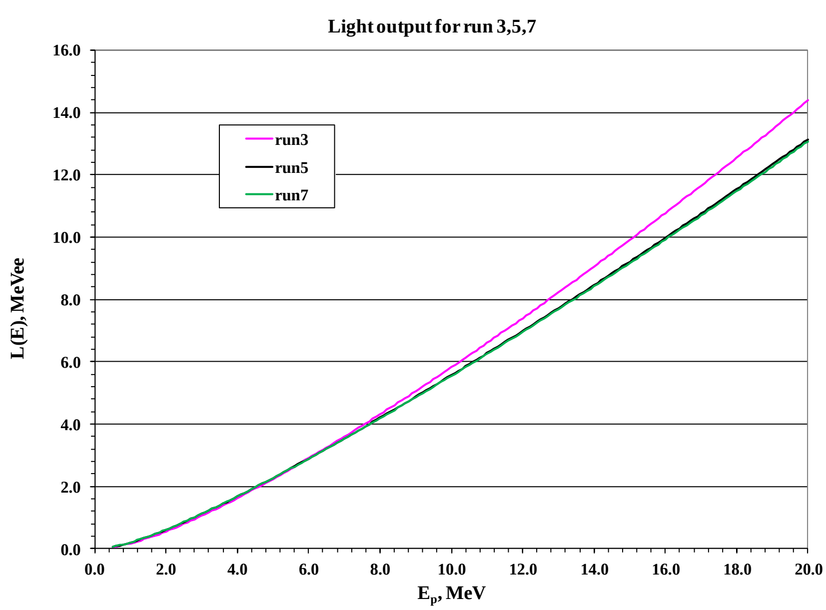


***Fig. 13****: Light output for runs 3, 5, and 7. Only fitted results are given.*

However, there is a difference (outside the uncertainties of estimation) between Run 3 (dynode 8), and Run 5 and 7 (dynode 10). It is much less than for Run 1 and 5 but the difference exists (see Fig. 13), and it increases with the increase of input neutron energy. Parameters and functions L(E) are rather close to each other. This fact may give us additional information about the influence of the L(E) function on the final result, and give an estimation of the accuracy of DYTH the method.

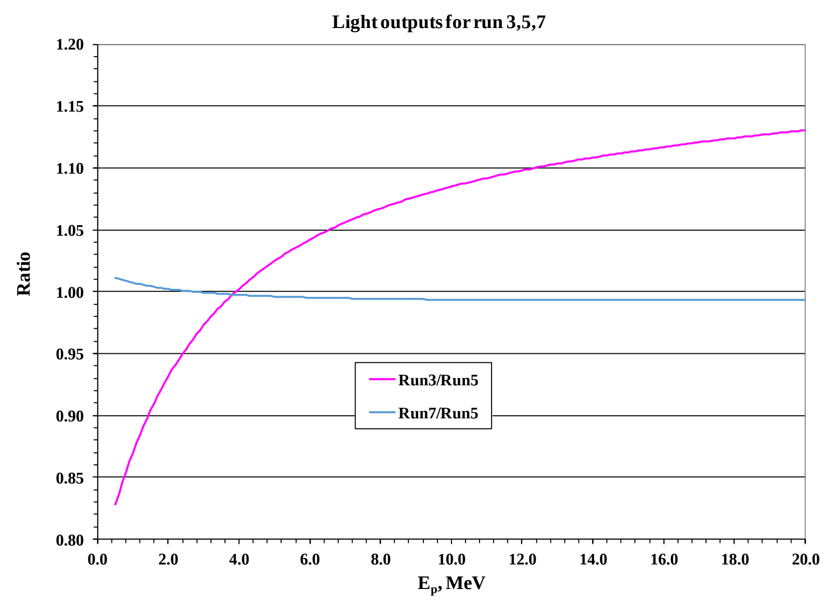


***Fig. 14:*** *Ratio Ri,5(E) = ΔLi/ΔL5 for run 3 (i=3) and 7 (i=7).*

The amount of protons counted after the interaction of neutrons with energy $E_0$ is proportional $\Delta L = L(E_0) - L(E_{min})$. So, the ratio $R_{ij}(E) = \Delta L_i/\Delta L_j$ (where i,j – is the run's number) may be used as an estimation of the uncertainties for DYTH the method. Ratios $R_{3,5}(E)$, and $R_{7,5}(E)$ for Runs 3,5 and 7 are shown in Fig. 14.

The direct comparison of model calculations for different L(E) functions does not give an adequate understanding about the accuracy of the method : for simulation of PH and the data selection we are using the same L(E) function.

However, the comparison demonstrated above, may serve as an important tool for estimation of the uncertainties of the method. In case of stable operation, and application of the same experimental setup (high voltage, the source of linear output, the same electronic units), the intrinsic uncertainties may be rather small ~ 1 %. If the deviation in light outputs is rather high, but no difference in spectrum shape is seen in different runs, that means that the measured L(E) function is *reality*. Then, the uncertainties of the data may be estimated from the data spread for different runs.

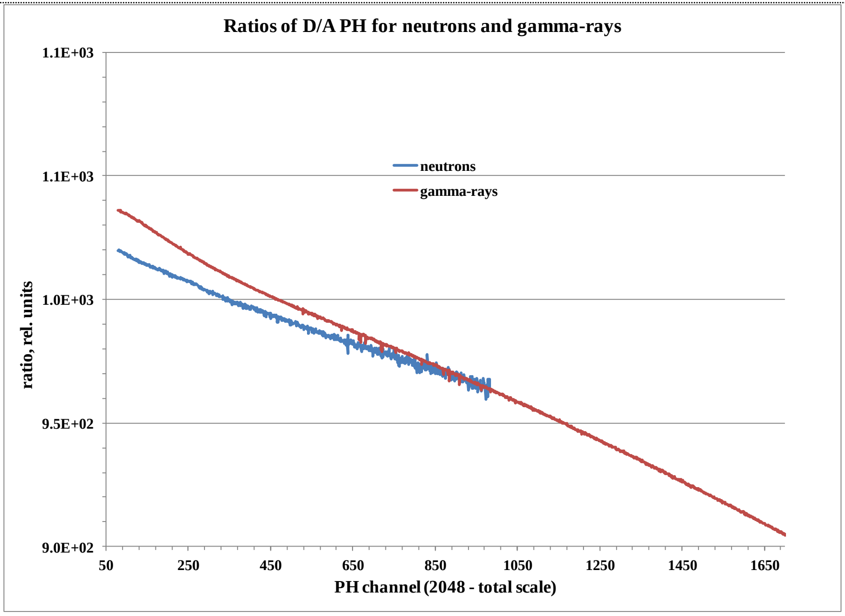


***Fig. 15****: Ratio of pulse height taken from 8th dynode and anode for neutrons and gamma-rays (run 3).*

Fig. 15 gives very useful information on which factors may provide important influence on the detector light output. The ratios of dynode and anode pulses for neutrons and gamma-rays are plotted versus of pulse height (dynode amplitude). The conclusion is as follows:

1. Instead of constant (value which should exists for ideal case) we see rather strong dependence on PH;
2. This is not a simple linear function;
3. The difference between neutrons and gamma-rays is clearly visible.

It was not the goal of these experiments to investigate these peculiarities and explain them. Therefore new efforts must concentrate on understanding the reasons. But one conclusion is obvious: *the light output of the detector is not only the property of the scintillator, but depends very much on the PMT characteristics and its operation*.

The typical dependence of energy resolution versus PH energy is shown in Fig. 16. The calculated results practically do not depend on this function for neutron energy > 2 MeV. The most sensitive is the low energy part of the spectrum < 2 MeV. However, due to very strong dependence for this range, we cannot calculate the efficiency with high accuracy, and this peculiarity provides the low energy limit for the DYTH method ~ 1.5 - 2 MeV.

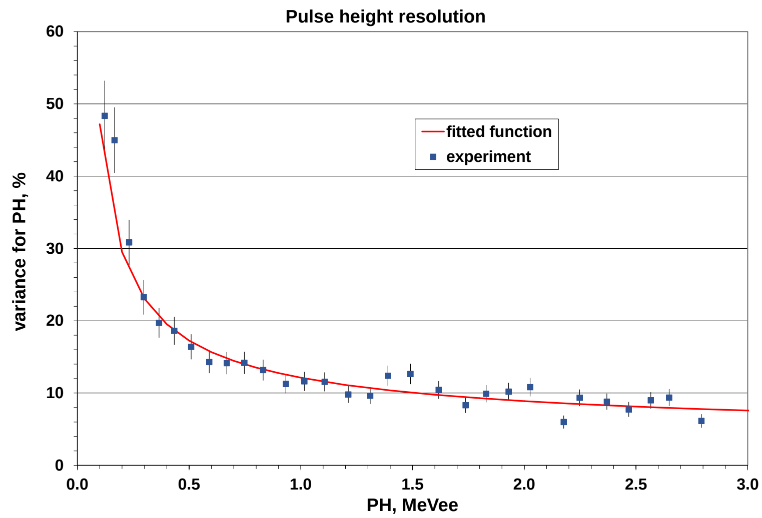


***Fig.16***: *Experimental and calculated resolution functions*

## 7. The efficiency of neutron counting and uncertainties of its calculation. Influence of different factors on final results (accuracy of method)

With the DYTH approach, experimental data and calculated efficiency (Monte Carlo simulation) were treated in the same way. Events simulated by the Monte Carlo model and collected during the experiment were selected according to equations 1-3 given above (in Section 2). Only simulated efficiency was applied for experimental spectra treatments.

The NEFF7-DYTH code was transformed from original NEFF7 [6]. The modernization includes: new approaches for L(E) calculations, and selection of simulated events according to Eqs. 1-3.

The detector model was the same as in the original program (Fig. 17). It consists of "housing" prepared from Al, with diameter $R_h$ and height $H_h$, and scintillator with diameter $R_s$ and height $H_s$. The scintillator and PMT was connected with "light guide" $R_l = R_s$, and height $H_l$. In our case $R_s = 5.6$ cm, $H_s = 5.0$ cm, $R_h = 5.9$ cm, $H_h = 5.2$ cm, $H_l = 1.2$ cm.

So far, several details were not taken into account: the structure of PMT, the "plastic pipe" in the "housing wall" which contains the extra liquid, and the semi-spherical light guide between scintillator and spherical PMT RCA 4522.

The "glass window" (h = 0.59 cm), and "plastic" was transformed into cylindrical "artificial material" $CH_{0.7}$. The density was assumed like a glass ( $SiO_2$, $\rho = 2.5$ g/cm$^2$). An additional amount of scattering material was added due to the "light guide" $C_5O_2H_8$. The length of this artificial material was estimated according to cross section which was assumed proportional $A^{2/3}$, and the total amount of atoms of the given material which is proportional 1/A. Finally, the "new light guide" was constructed with $\rho = 2.5$ g/cm2, l = 1.2 cm, H/C ratio 0.7.

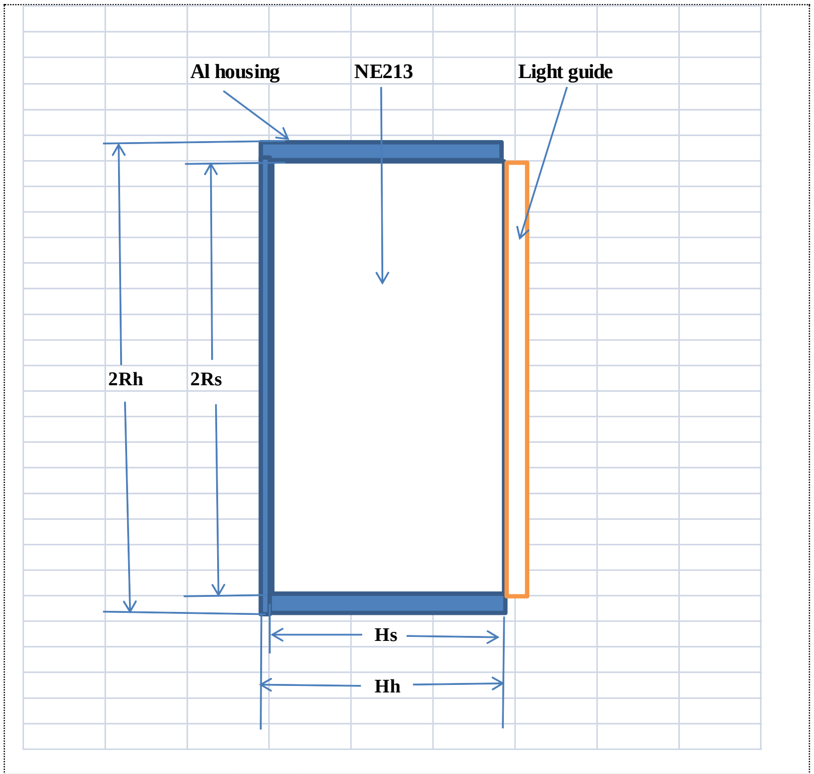


*Fig. 17:. The model of neutron detector.*

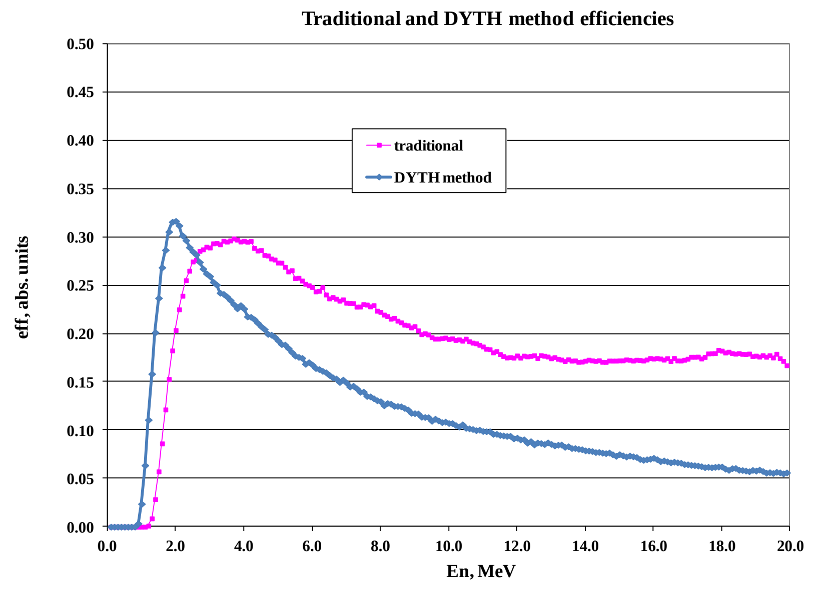


***Fig.18**: Calculated efficiencies for DYTH and fixed threshold (traditional approach).*

Efficiencies of the detector calculated both with the traditional and DYTH methods are shown in Fig. 18. At high energy, the DYTH method (in comparison with the traditional approach) demonstrates smooth function connected only with (n,p) scattering on hydrogen. There is not any structure (or "waves") at neutron energy > 10 MeV. This is the main goal of the new approach – keep (n,p) scattering only as a main component. Nevertheless, the structure connected with C(n,n) resonances (see Fig. 19) should be visible.

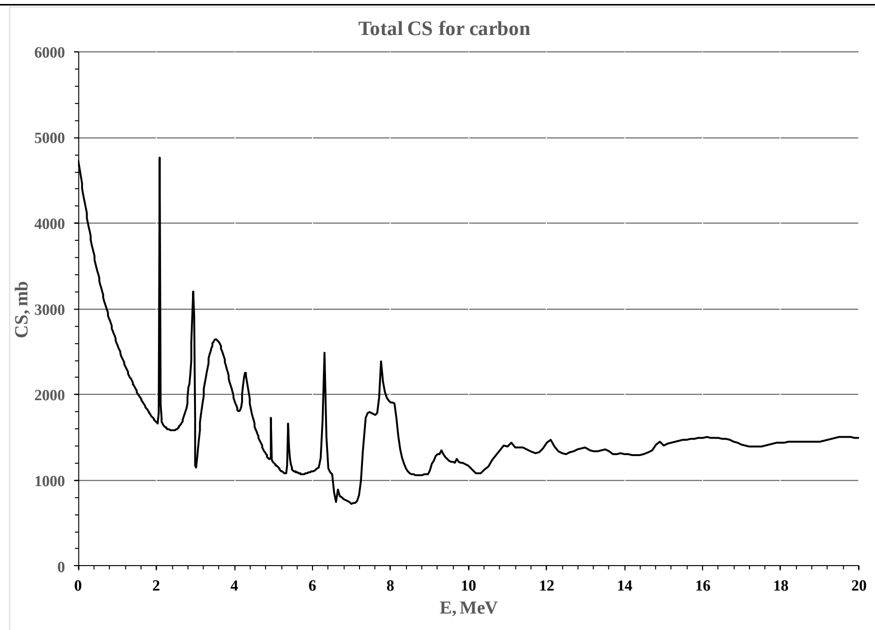


***Fig.19***: *Total neutron cross section for C.*

The detector efficiency may be calculated with a simple analytical Equation:

$$\varepsilon(E) = \alpha \frac{\Sigma p}{\Sigma t}(1 - \exp(-\Sigma t \cdot H)) \qquad (6)$$

where $\Sigma_p = \sigma_p n_p$, $\Sigma_c = \sigma_c n_c$, $\Sigma_t = \Sigma_p + \Sigma_c$, $\alpha$ – is counted part of scattering protons (in our case $\alpha = 0.5$).

The efficiency calculated with Eq.6 is shown in blue in Fig. 20 together with DYTH method calculations. In the MC simulation the same scintillator height was assumed H = 5cm but with different radius R = 5 cm, (this is the size of our real detector), and with R = 0.5cm. The resolution parameters were the same for both sizes of scintillators.

The MC simulation for R = 0.5 cm demonstrates the structure connected with C cross sections. The "broad" resonances at ~ 3 - 4 MeV and ~ 8 MeV is clearly visible. This "fluctuation function" is very close to analytical approach Eq.6, and connected with self-absorption or removing of some amount of neutrons from input beam.

But the function is smooth for the "big" scintillator. Neutrons scattered on C, due to the big radius of the scintillator cannot be removed from the "counting process". They will be counted again due to multiple scattering. Due to this, the efficiency is a smooth function. The structure effect in narrow resonances may be lost due to resolution of the detector. However, one may expect some visible structure effect in broad resonances. It seems that the “structure effect” at energies ~ 4 and ~ 8 MeV should be sensitive to angular distribution of neutrons scattered on carbon.

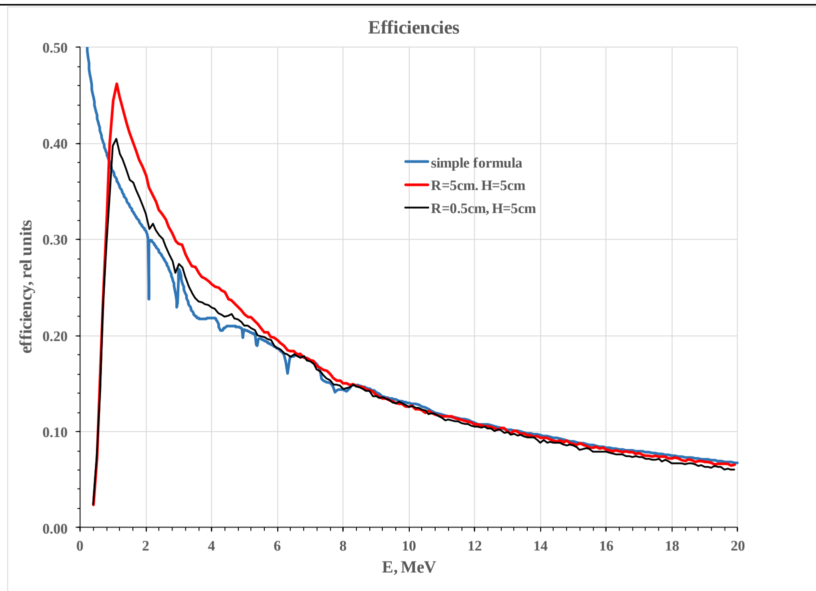


***Fig.20****: Calculated efficiencies with different assumptions.*

Of course, the model of the detector should simulate all processes as close to reality as possible. Modifications of the NEFF7 code include detector environment parts which are placed close to the scintillator where they have the highest impact on the calculated result.

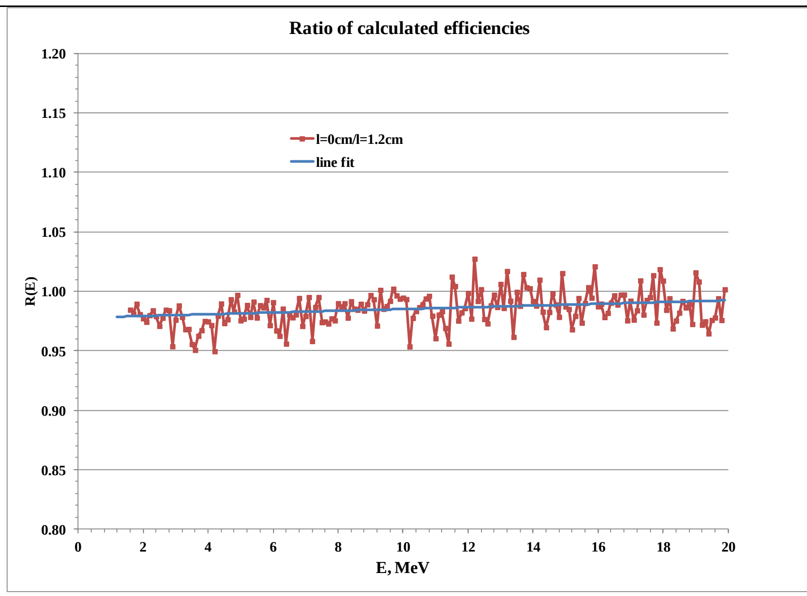


***Fig.21****: Ratio of calculated efficiencies with different lengths of “light guides” (l=0 cm and l=1.2cm).*

The rather artificial “light guide” was used in MC model. The influence of this simplification was investigated with additional calculations. The detector efficiencies were calculated for two lengths of the “light guide” l=0 cm and l = 1.2 cm. The ratio of these functions is shown in Fig. 21. The fitted linear function y = 0.9778 + 0.0007 E.

The incorporation of hydrogen in the “light guide” also has very little influence. It is important (may be) only for the energy range ~ 4 MeV, where “structure” was visible (Fig. 22).

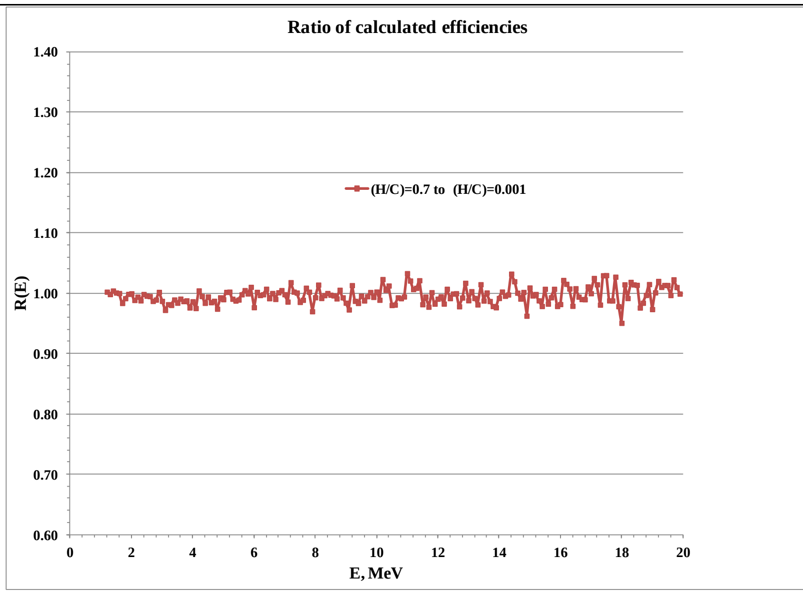


***Fig.22****: Ratio of calculated efficiencies with different contribution of H in “light guide” (H/C=0.7 and H/C=0.001).*

The cylindrical surface of the detector housing is Al. However, in reality there is a plastic pipe with liquid for temperature compensation inside the Al-wall. Taking into account the result of “light guide” investigation, the influence of this transformation should be rather small.

On the basis of these arguments (see also Section 6) one may conclude that efficiency of the scintillator detector, operated with the DYTH method, may be estimated with accuracy ~ 2% in the whole energy range where the light output function may be derived directly from the experiment (without extrapolation). The incorporation of a more realistic model for MC simulation may even reduce this uncertainty.

## 8. Experimental data analysis

Experimental data analysis for each run consists of the following steps:

1. Analysis of gamma-ray spectra for scale calibration;
2. Estimation of time channel width from delay event spectra. Experiment with numerical generator;
3. Collection of some events for estimation of correction for the time shift versus PH;
4. Estimation of “cut” between neutrons and gamma-rays versus PH for neutron-gamma discrimination;

5. Evaluation of zero-time position (prompt gamma-ray), and time resolution for each short run;
6. Check the gain stability for each short run;
7. Collection of TOF events to construct the RF matrix, energy resolution, light output (electron energy) versus proton energy;
8. Fit parameters for estimation functions L(E), σ(E);
9. Monte Carlo simulation of the detector efficiency;
10. Calculation of the "bin" and "time resolution correction";
11. Sorting of events according to the DYTH method, and taking into account the gain correction (if necessary), "bin-time resolution" correction, detector efficiency, neutron-gamma selection. The calculation of the energy spectrum and its uncertainties, in absolute units and relative to Mannhart's standard.

Points 1 – 7 are evaluated in traditional event analysis and only after efficiency calculation (p 8) the DYTH method is applying for data sorting and final data evaluation.

The experimental spectrum S(E) is connected with "real" data $S_0(E)$ (normalized to unit) by Equation:

$$S(E) = S_0(E) \cdot N \cdot \frac{\nu}{4\pi} \cdot \varepsilon(E) \qquad (7)$$

$$N = T\Omega N_f$$

Where ν = 3.759 prompt neutron multiplicity, ε(E) – efficiency of neutron detector, T total time of experiment, Ω solid angle of detector, $N_f$ fission fragment count rate.

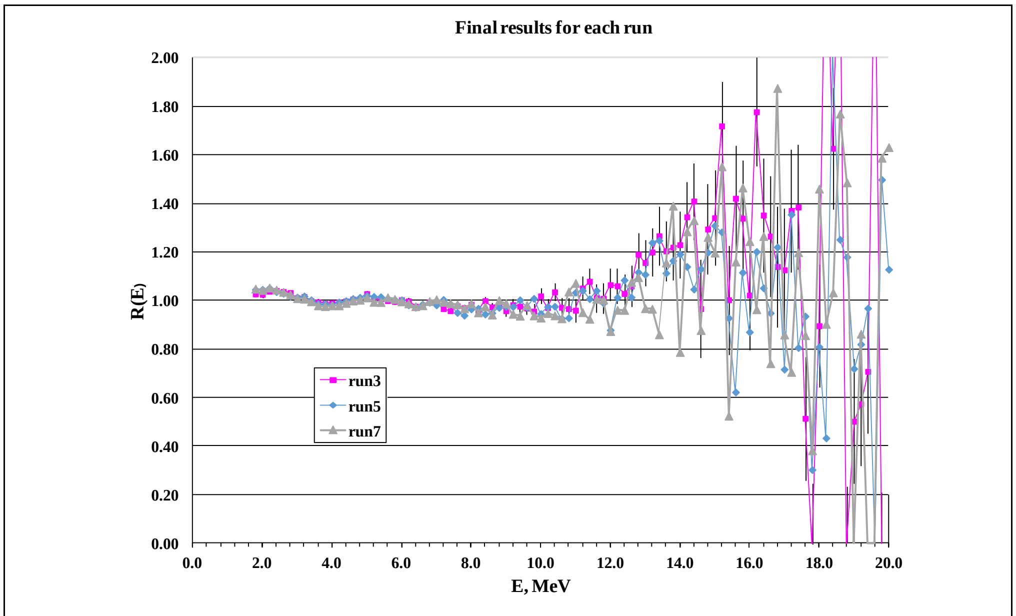


***Fig.23**: Ratio of experimental data for Runs 3,5, and 7 to $^{252}$Cf standard.*

After this normalization, the ratio R(E) = S(E)/$S_0$(E) was estimated. The average value <R> and its standard deviation δR are listed in Table 4.

Table 4. Average ratio for energy range 2 - 8 MeV.

| | <R> | δR |
|---|---|---|
| run3 | 1.019 | 0.029 |
| run5 | 0.993 | 0.016 |
| run7 | 0.974 | 0.023 |

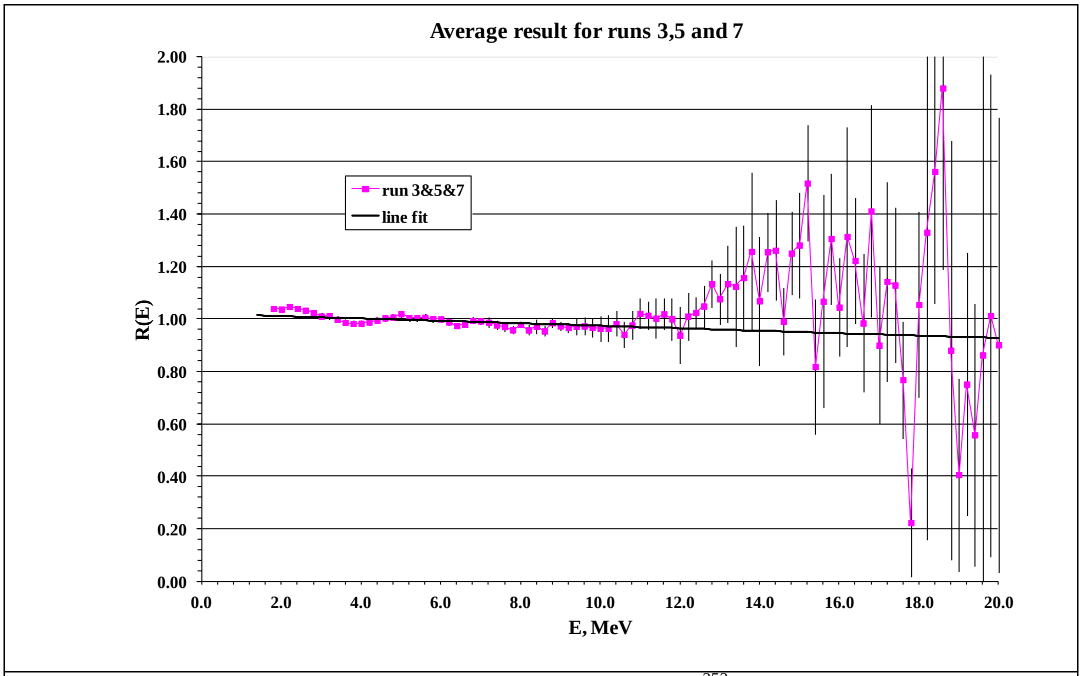


***Fig.24:*** *Average ratio for Runs 3,5, and 7 to* $^{252}$*Cf standard.*

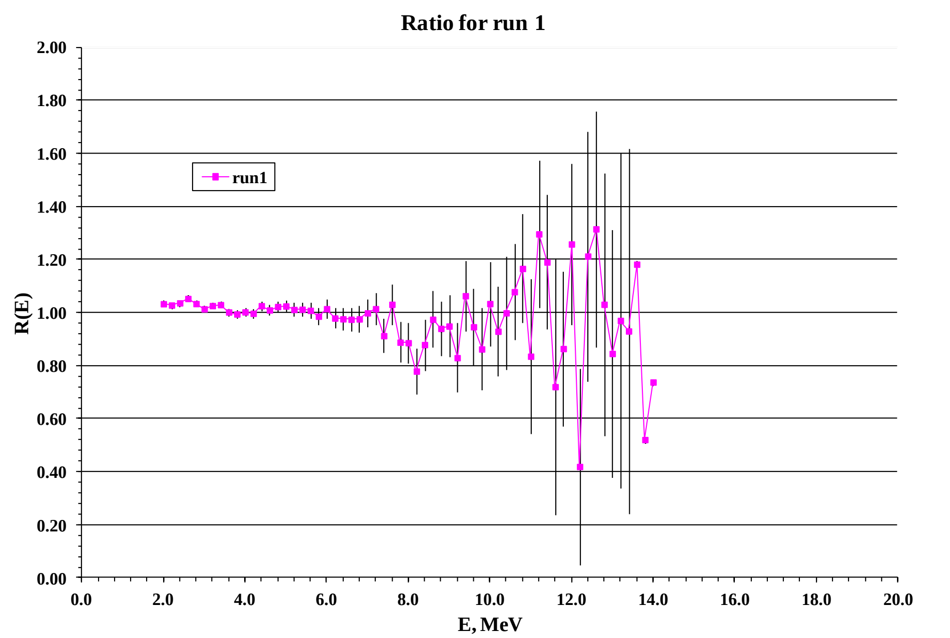


***Fig. 25:*** *Ratio to $^{252}$Cf standard for Run 1.*

Data with an additional normalization (table 4) were used in following discussion. However, one should conclude that intrinsic normalization (eq. 7) looks reasonably well.

## 9. The comparison of all measured data

All experimental data as ratio to the $^{252}$Cf standards are collected on Figs. 23-25. The following peculiarity should be highlighted.

The experimental data measured during Runs 3,5, and 7 are in very good agreement. Independent measurements of all important parameters and characteristics were realized for each run: light output function, flight path, time channel width, "cut" for neutron-gamma discrimination, zero-time estimation.

So, one may conclude that there is an invisible conflict between each measured function and "reality". The strong deviation of the L(E) function for Run 3 (see Fig. 14) is measured reality. Its application for experimental data analysis gave the "real" spectrum shape, which was confirmed by experimental results from Run 5,7.

All data were extrapolated to standard energy scale (step 0.2 MeV). Therefore, one may use a rather simple, but most effective method for the estimation of uncertainties in the final results. The spectrum for each energy point was calculated as average between Runs 3,5, and 7. The error bars were found as a standard deviation of data for each Run.

This data and uncertainties are given in Fig. 24 as a ratio. According to all these runs, the average function is close to the $^{252}$Cf standards. New data confirm Mannhart's evaluation in energy range 3-12 MeV inside the accuracy of standards (see Table 5). The linear function

$$f(E) = s_o + s_1 \cdot E \qquad (8)$$

was fitted to experimental points in the energy range 3 - 12 MeV, The residual $\chi^2$ = 1.8, $s_o = 1.0206 \pm 0.0033$, $s_1 = -(0.0046\pm0.0007)$.

A more detailed comparison may be carried out on the basis of data listed in Table 5.

Table 5. Average spectrum and its standard deviation for ~1 MeV energy intervals from 1.8 MeV to 20 MeV. $E_1$-$E_2$ – averaging interval, <R> average ratio to Mannhart evaluation, dR – standard deviation of average values estimated for each run.

| $E_1$-$E_2$ MeV | <R> | dR | Mannhart uncertainties | Line function, eq. 8 |
|---|---|---|---|---|
| 1.8-3.0 | 1.034 | 0.003 | 0.012 | 1.009 |
| 3.0-4.0 | 0.996 | 0.004 | 0.012 | 1.004 |
| 4.0-5.0 | 1.000 | 0.005 | 0.014 | 1.000 |
| 5.0-6.0 | 1.007 | 0.004 | 0.016 | 0.995 |
| 6.0-7.0 | 0.988 | 0.003 | 0.016 | 0.990 |
| 7.0-8.0 | 0.978 | 0.009 | 0.018 | 0.986 |
| 8.0-9.0 | 0.971 | 0.008 | 0.021 | 0.981 |
| 9.0-10 | 0.970 | 0.017 | 0.024 | 0.976 |
| 10-11 | 0.975 | 0.012 | 0.029 | 0.972 |
| 11-12 | 1.000 | 0.029 | 0.030 | 0.967 |
| 12-13 | 1.039 | 0.052 | 0.050 | 0.963 |
| 13-14 | 1.137 | 0.102 | 0.100 | 0.958 |
| 14-15 | 1.186 | 0.072 | 0.120 | 0.953 |
| 15-16 | 1.173 | 0.144 | 0.150 | 0.949 |
| 16-17 | 1.147 | 0.140 | 0.200 | 0.944 |
| 17-20 | 0.961 | 0.058 | 0.300 | |

Absolute spectrum and uncertainties are given in Table 6.

Table 6. Experimental $^{252}$Cf spectrum $S_{0exp}(E)$, and its uncertainties $dS_{0exp}(E)$.

| E, MeV | $S_{0exp}(E)$, 1/MeV | $dS_{0exp}(E)$, 1/MeV | E, MeV | $S_{0exp}(E)$, 1/MeV | $dS_{0exp}(E)$, 1/MeV |
|---|---|---|---|---|---|
| 2.00E+00 | 2.440E-01 | 2.74E-03 | 1.12E+01 | 7.301E-04 | 4.00E-05 |
| 2.20E+00 | 2.247E-01 | 1.86E-03 | 1.14E+01 | 6.312E-04 | 4.89E-05 |
| 2.40E+00 | 2.028E-01 | 8.47E-04 | 1.16E+01 | 5.605E-04 | 3.36E-05 |
| 2.60E+00 | 1.823E-01 | 6.83E-04 | 1.18E+01 | 4.807E-04 | 3.85E-05 |
| 2.80E+00 | 1.629E-01 | 1.23E-03 | 1.20E+01 | 3.942E-04 | 4.30E-05 |
| 3.00E+00 | 1.444E-01 | 3.22E-04 | 1.22E+01 | 3.709E-04 | 3.34E-05 |
| 3.20E+00 | 1.297E-01 | 7.76E-04 | 1.24E+01 | 3.282E-04 | 2.03E-05 |
| 3.40E+00 | 1.142E-01 | 3.52E-04 | 1.26E+01 | 2.937E-04 | 2.35E-05 |
| 3.60E+00 | 1.005E-01 | 7.11E-04 | 1.28E+01 | 2.771E-04 | 2.49E-05 |
| 3.80E+00 | 8.918E-02 | 5.34E-04 | 1.30E+01 | 2.297E-04 | 2.25E-05 |
| 4.00E+00 | 7.926E-02 | 4.31E-04 | 1.32E+01 | 2.112E-04 | 3.12E-05 |
| 4.20E+00 | 7.062E-02 | 5.65E-04 | 1.34E+01 | 1.827E-04 | 4.19E-05 |
| 4.40E+00 | 6.293E-02 | 3.12E-04 | 1.36E+01 | 1.641E-04 | 3.28E-05 |
| 4.60E+00 | 5.613E-02 | 2.38E-04 | 1.38E+01 | 1.556E-04 | 4.67E-05 |
| 4.80E+00 | 4.973E-02 | 2.50E-04 | 1.40E+01 | 1.153E-04 | 2.83E-05 |
| 5.00E+00 | 4.440E-02 | 3.47E-04 | 1.42E+01 | 1.181E-04 | 1.77E-05 |
| 5.20E+00 | 3.858E-02 | 4.30E-04 | 1.44E+01 | 1.035E-04 | 1.98E-05 |
| 5.40E+00 | 3.394E-02 | 3.76E-04 | 1.46E+01 | 7.088E-05 | 9.10E-06 |
| 5.60E+00 | 2.990E-02 | 2.10E-04 | 1.48E+01 | 7.797E-05 | 1.25E-05 |
| 5.80E+00 | 2.615E-02 | 1.37E-04 | 1.50E+01 | 6.962E-05 | 1.39E-05 |
| 6.00E+00 | 2.293E-02 | 8.44E-05 | 1.52E+01 | 7.184E-05 | 1.58E-05 |
| 6.20E+00 | 1.990E-02 | 1.60E-04 | 1.54E+01 | 3.374E-05 | 8.68E-06 |
| 6.40E+00 | 1.721E-02 | 1.38E-04 | 1.56E+01 | 3.836E-05 | 1.56E-05 |

| E, MeV | $S_{0exp}(E)$, 1/MeV | $dS_{0exp}(E)$, 1/MeV | E, MeV | $S_{0exp}(E)$, 1/MeV | $dS_{0exp}(E)$, 1/MeV |
|---|---|---|---|---|---|
| 6.60E+00 | 1.517E-02 | 1.21E-04 | 1.58E+01 | 4.090E-05 | 1.02E-05 |
| 6.80E+00 | 1.349E-02 | 1.08E-04 | 1.60E+01 | 2.850E-05 | 5.36E-06 |
| 7.00E+00 | 1.181E-02 | 1.37E-04 | 1.62E+01 | 3.121E-05 | 1.31E-05 |
| 7.20E+00 | 1.029E-02 | 2.01E-04 | 1.64E+01 | 2.530E-05 | 6.07E-06 |
| 7.40E+00 | 8.919E-03 | 1.54E-04 | 1.66E+01 | 1.775E-05 | 4.68E-06 |
| 7.60E+00 | 7.758E-03 | 1.43E-04 | 1.68E+01 | 2.217E-05 | 8.95E-06 |
| 7.80E+00 | 6.706E-03 | 1.15E-04 | 1.70E+01 | 1.232E-05 | 3.70E-06 |
| 8.00E+00 | 5.993E-03 | 7.30E-05 | 1.72E+01 | 1.363E-05 | 5.18E-06 |
| 8.20E+00 | 5.136E-03 | 1.03E-04 | 1.74E+01 | 1.173E-05 | 3.47E-06 |
| 8.40E+00 | 4.561E-03 | 1.26E-04 | 1.76E+01 | 6.951E-06 | 1.56E-06 |
| 8.60E+00 | 3.918E-03 | 7.84E-05 | 1.78E+01 | 1.765E-06 | 3.67E-07 |
| 8.80E+00 | 3.540E-03 | 7.08E-05 | 1.80E+01 | 7.243E-06 | 2.56E-06 |
| 9.00E+00 | 3.059E-03 | 6.12E-05 | 1.82E+01 | 7.960E-06 | 9.33E-06 |
| 9.20E+00 | 2.659E-03 | 5.29E-05 | 1.84E+01 | 8.140E-06 | 4.07E-06 |
| 9.40E+00 | 2.337E-03 | 7.70E-05 | 1.86E+01 | 8.533E-06 | 5.90E-06 |
| 9.60E+00 | 2.048E-03 | 6.76E-05 | 1.88E+01 | 3.481E-06 | 2.78E-06 |
| 9.80E+00 | 1.780E-03 | 6.52E-05 | 1.90E+01 | 1.399E-06 | 5.16E-07 |
| 1.00E+01 | 1.552E-03 | 7.41E-05 | 1.92E+01 | 2.250E-06 | 1.12E-06 |
| 1.02E+01 | 1.358E-03 | 6.79E-05 | 1.94E+01 | 1.453E-06 | 7.28E-07 |
| 1.04E+01 | 1.210E-03 | 5.91E-05 | 1.96E+01 | 1.951E-06 | 2.92E-06 |
| 1.06E+01 | 1.013E-03 | 5.07E-05 | 1.98E+01 | 1.988E-06 | 1.83E-06 |
| 1.08E+01 | 9.199E-04 | 5.06E-05 | 2.00E+01 | 1.535E-06 | 1.33E-06 |
| 1.10E+01 | 8.410E-04 | 4.81E-05 | | | |

It is worth noting that some peculiarities are visible (Figs. 24, 25):

1. There is the deep minimum ~ 15% at 8 MeV according to Run 1 (outside uncertainties).
2. The broad minimum ~ 1.5 % is clearly visible at ~ 4 MeV, and the small minimum at ~ 6 MeV;
3. There is ~ 3 % excess of neutrons in the energy range < 3 MeV;
4. There is a linear deviation from the standard which is outside of the uncertainties estimated here and given in Tables 5,6;
5. There is a "broad bump" at energy > 12 MeV at the edge of the uncertainties band (see Figs 23,24).

The setup of Run 1 is in comparison different from other runs. The same detector type was applied. However, three identical detectors were placed in the triangle tops, and touching each other in Run 1. Events counted in more than one detector were collected separately. So-called "cross talk" correction was applied for this assembly. The carbon total cross section has a broad maximum at neutron energy ~ 8 MeV. However, we cannot see the similar tendency for Run 3,5, and 7 where only one detector was applied. So the "cross talk" effect should be responsible for this minimum.

The carbon cross section is 1.9 b and H(n,p) is 1.1 b at 8 MeV. This minimum cannot be connected with the secondary process after (n,p) scattering in the first detector. The DYTH selection collects protons in the energy range 4-8 MeV. So the scattering neutrons cannot see this resonance in C(n,n) reaction. One may assume that the first scattering happened on carbon in the first detector. After this scattering, the neutron changes direction and moves into the second and third detector. This scattered neutron may produce a second interaction on H in the first detector, and the first interaction on hydrogen in detectors two or three. In this case this event will be rejected. The higher C cross section provides higher "cross talk" correction and as a consequence a minimum in this energy range. This may explain why there is no "strong" structure at ~ 8 MeV for a single detector.

The minimum at ~6 MeV may be explained as a self-absorption effect due to the narrow resonance on C with a maximum at 6.3 MeV (2.49 b). The similar explanation may be valid for broad structure (minimum) at ~ 4 MeV. The problem is that the calculated efficiency (see Fig. 20) does not reproduce these structures. It may be connected with the different angular distribution for these resonances which are used in the Monte Carlo code and exist in reality.

In Run 1 and Runs 3-7, there is a neutron excess at energy < 3 MeV. This may be connected with an additional scattering on the detector environment. With this explanation it is rather strange to see practically the same contribution with an additional 2 detectors placed very close to each other (Run 1) and the results for Runs 3-7 (only one detector).

Detector assembly was placed in a distance of ~ 1 m from the collimator exit in Run 1. In case of Run 3-7 this distance was ~ 0.3 m. The diameter of the collimator was ~30 cm, and the contribution of scattering on the collimator in Run 3-7 should be higher. However, the only direct simulation of the detector's environment (collimator, holder, PMT, and so on) may give a correct answer about the nature of these neutrons, and allow to predict the detector efficiency with higher accuracy. Of course, one may assume that these neutrons are reality, and the standard spectrum also requires an additional correction for this energy range.

The linear deviation of the measured spectrum from the Cf standards may be explained as systematical uncertainty of the DYTH method or deviation of the Cf standards from reality. There are no arguments for choice.

The broad maximum was measured for the energy range 12-18 MeV. The data from Run 7 are shifted and support this deviation from ~ 15 MeV. This fact may be used as an argument that this effect has a “methodical nature”. The light output was estimated from Cf spectrum, and experimental points were available for energy range < 12 MeV for Runs 3,5, and 7. The extrapolation was used for higher energy. The systematical deviation of experimental points for higher energy may be connected with this procedure. The extrapolated function may contradict to the real one for this energy interval.

## 10. Conclusions about Cf standard shape and uncertainties of DYTH method

According to Table 5, this experimental result confirms Mannhart’s evaluation within its uncertainties in the energy range 3 - 20 MeV.

However, estimated uncertainties of new experimental results are less than the error bars accepted for the Cf standard.

There are two possibilities:

1. The experimental data are correct (systematical errors less than uncertainties of standard spectrum) and the Cf standards should be re-evaluated taking into account recommendation of this paper (for example the linear deviation from the standard spectrum).
2. The deviation from the standard spectrum is due to the systematical error of the DYTH method. In this case one may estimate the uncertainties of the method.

Taking into account the above discussion, and data listed in Table 5 one may estimate the uncertainties of the DYTH method (see table 7).

Table 7. Estimated uncertainties for the DYTH method.

| $E_1$-$E_2$, MeV | dS/S, % |
|---|---|
| < 3 | 3.0 |
| 3-7 | 2.0 |
| 7-10 | 2.5 |
| 10-13 | 4.0 |

Detailed simulation of neutron scattering on the detector environment may reduce uncertainties at low energy. The application of the DYTH method with high accuracy is possible only in the energy range where the light output function may be measured by experiment.
The absolute Cf spectra are shown in Fig. 26, where experimental data are compared with Cf standard and the theoretical result. The model calculation was realized with code FIssion Neutron Emission (FINE).

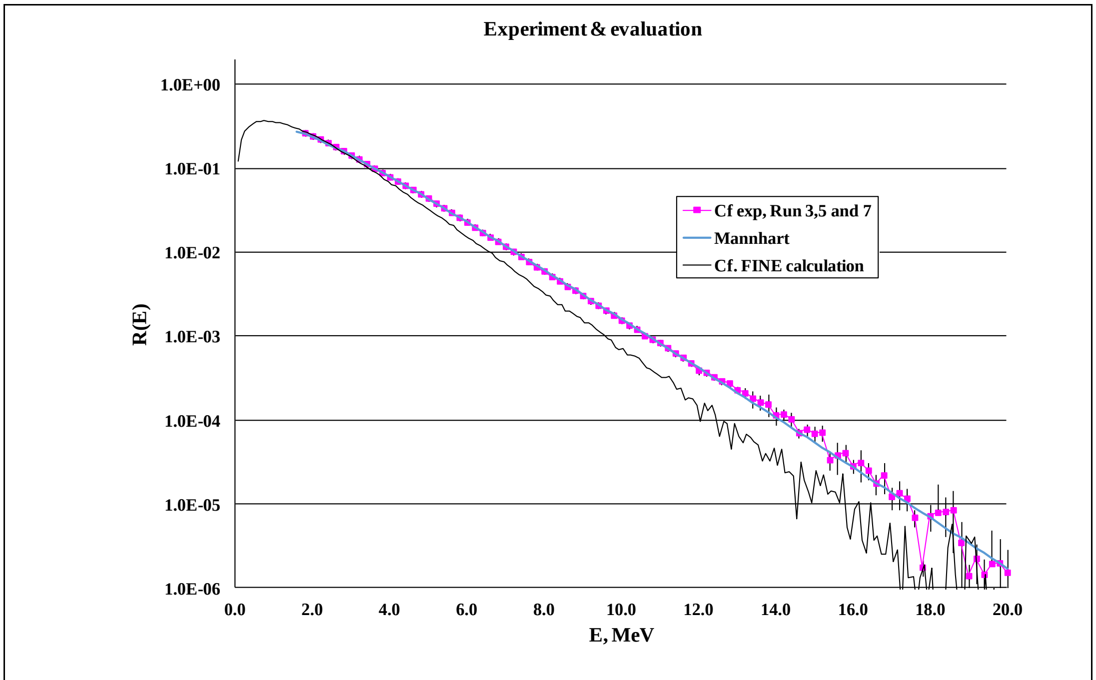


*Fig.26 Absolute 252Cf spectrum. Points – experimental data, shown on Fig. 24 as a ratio, blue line – Cf-standard, black line - theoretical calculation with code FINE.*

The details of this calculation may be found in Ref [11]. It should be noted, that this model includes a detailed simulation of fission fragment distribution versus kinetic energy, masses, charge and excitation energy. Neutron emission was possible if the excitation was higher than the neutron binding energy for a particular fragment. The difference between spectrum shape (model result and experimental data) is the point for separate discussion.

It is important to highlight here, that the spectrum shape is the smooth function without any "bump" or fluctuations. It is a good achievement, to see the fission neutron spectrum changing with 6 orders of magnitude.

## 11. Final conclusions and recommendations

1. The $^{252}$Cf standard PFNS was verified in the energy range 2 - 20 MeV. Inside the uncertainties of the standard spectrum its shape was confirmed. No peculiarities were observed at high energies.
2. There are some hints that the standard spectrum may be corrected a bit. However, additional investigations should be carried out to verify this correction.
3. This was the first application of the DYTH method after publication [4]. The investigation confirmed that this is a unique method to measure neutron spectra in the energy range 2 - 20 MeV (or higher) with the highest possible accuracy.
4. Detailed simulation of neutron scattering on the detector environment (and detector itself) by means of the Monte Carlo method is very important to estimate detector efficiency with high accuracy. There are some materials with nuclei with A = 50 - 60 (Fe, Cu, etc.) around the detector (detector holder, PMT dynodes, and so on). The share of these materials is rather small, but neutron scattering on these materials may give contribution comparable with function Eq 8.

5. Important advantages of the DYTH method are: improvement of time resolution, considerable reduction of the background, using mainly (n,p) scattering for neutron counting in the whole energy range for calculating efficiency with high accuracy. All these factors (and method itself) may be realized only if the light output L(E) function will be measured in the whole energy range selected for investigations. Any extrapolation may provide systematic uncertainties.
6. Uncertainties of the DYTH method at low energy, mainly connected (assumption) with scattering on the environment (collimator) may be reduced if the TOF method with Cf source in the low energy range < 8 MeV will be applied for the measurement of detector efficiency. The efficiency for energy range >8 MeV will be estimated by means of MC simulation.

**Acknowledgement**

I am grateful to T. Massey, D. Carter, and S. Grimes for assistance during the experiment realization, and interesting discussions.

**References**

[1] W. Mannhart, IAEA-TECDOC-410, (1987), p158.

[2] P. Staples, J.J. Egan, et al, Nucl. Phys A591, 1995, 41.

[3] N. Kornilov, T. Massey, S. Grimes, et al, report for ND2013, NY, 2013.

[4] N. Kornilov, S. Grimes, T. Massey, Scintillation neutron detector with dynamic threshold, Report for NEMEA-7/CIELO workshop, 5-8 Nov, 2013.

[5] J.D. Brandenberger and T.B.Grandy, NIM 93 (1971) 495-508.

[6] G. Dietze, H. Klein, Nucl. Instr. and Meth. 193 (1982), 549. G. Dietze and H. Klein, PTB-ND-22 Physikalisch- Technische Bundesanstalf, 1982.

[7] N. Kornilov, I. Fabry, et al, “Total characterisation of neutron detector with Cf source and a new light output determination”, NIMPR A599 (2009), 226-233.

[8] G. Randers-Pehrson, et al., Nucl. Instr. and Meth. 215, 433(1983).

[9] www.mesytec.com, MPD-4 neutron-gamma discriminator.

[10] N.V. Kornilov, T.N. Massey, S.M. Grimes, D. Sayer, C.E. Breint, D. E. Carter, et al, Energy scale calibration and off-line gain stabilization of scintillation neutron detectors, report for ND2013 conference, NY 2013 (available at: http://www.researchgate.net/profile/N_Kornilov ).

[11] N.V. Kornilov, Fission neutrons: experiments, evaluation, modeling and open problem, Springer, 2015, ISBN978-3-319-07132-9.

Nuclear Data Section
International Atomic Energy Agency
Vienna International Centre, P.O. Box 100
A-1400 Vienna, Austria

E-mail: nds.contact-point@iaea.org
Fax: (43-1) 26007
Telephone: (43-1) 2600 21725
Web: http://www-nds.iaea.org